PAPER L

MIGRATION OF CROSSWELL SEISMIC DATA: FIELD DATA CASE

Le-Wei Mo and Jerry M. Harris

ABSTRACT

The prestack reverse-time migration scheme described in Mo and Harris (1993a) is applied to a field crosswell dataset, recorded in west Texas.

It is shown that proper prestack reverse time migration, filtering, and stacking of crosswell seismic data give high-quality reflectivity images of multi-elastic wavemodes of P-P, P-S, S-P, and S-S.

DESCRIPTION OF SITE

Our field data were recorded in a west Texas carbonate reservoir between two wells of 184 ft apart and over a depth interval of 500 ft. The two wells are roughly vertical (Lazaratos, 1993). Data were acquired using the piezoelectric source and a hydrophone array. Field operations were distinguished by the fact that nearly 40,000 seismic traces were recorded in about two days using the new acquisition method of recording on-the-fly, where the source is continuously moving while being fired. This fast recording technique guarantees that all the elastic wave modes signals are recorded without aliasing, even though the tube wave is slightly aliased. What is more important, source depth control was accurate enough to test the migration algorithm. The reservoir pay zone is from depth of 2850 ft to 2950 ft. The dataset consisted of 201 shots and 178 receivers. The source and receiver depth intervals are both 2.5 ft. A more detailed description of the geology and the data acquisition was given in Harris et al. (1992).

DESCRIPTION OF FIELD DATA

Figure 1 is an unprocessed common receiver gather. Even though it is scalar data, it contains a rich variety of elastic wave modes, P-P, P-S, S-P, and S-S, the bandwidths of which range from a few hundred Hertz up to a few thousands Hertz. The generation of these elastic wavemodes is explained by the following fact. In a fluid-filled borehole, the pressure variations produced by the expansion and contraction of the piezoelectric source are coupled at the source borehole wall to the drilled formation to generate radiated P and S waves. These P and S waves are reflected, diffracted, converted in

the formations. The resulting P-P, P-S, S-P, and S-S elastic wave modes are coupled at the receiver borehole wall into pressure variations in the receiver borehole to be recorded.

BACKGROUND VELOCITY MODEL

Figure 2 shows a vertically and horizontally variable but smooth background velocity model, whose velocity ranges from 15000 ft/s to 21000 ft/s. The grid size is 480 x 148. This model is derived from the result of transmission traveltime tomography (Van Schaack et al, 1992) after some smoothing to attenuate the effects of possible artifacts in the tomogram. The portion above 2650 ft and the portion below 3150 ft are made by extrapolating the original tomogram velocity model. The two wells are separated by 184 ft. Assuming a constant Poisson's ratio, the S-wave velocity is derived as a factor 1/1.8 of the P-wave tomogram velocity. These smooth P- and S-wave velocity models are used as the background models of migration and used to compute the imaging conditions of migration.

The reason that tomogram is an accurate background velocity model for migration is explained by migration dephasing (Mo, 1992).

PREPROCESSING OF FIELD DATA

Figure 3 is the same common receiver gather as Figure 1, having been processed in common offset sections to remove the direct P waves and direct S waves.

Our migration algorithm was developed using a point-source in a 2-D space that is equivalent to a line-source perpendicular to the survey plane in a 3-D space in which the geological structures are invariant along the line-source direction (2-D geology). Wapenaar et al (1990) gave a method for transforming point-source data into line-source data in the surface reflection configuration. For simplicity, this elaborate procedure was replaced by a simple scaling of the data by a power of the recording time. A theoretical justification for this approximation can be found in Claerbout (1985). 2-D geometrical spreading in a constant velocity medium differs by $\sqrt{t}$ from the 3-D spreading. In this dataset, we have made the 3-D to 2-D amplitude adjustment by applying a time scaling of $\sqrt{t}$.

There are some blank traces in the data. And the spatial sampling interval is not fine enough for wave propagation computed by finite differences. Thus the data must be interpolated.

FIELD DATA MIGRATION

The data of Figure 3 contain various elastic wavemodes. There are P-P wave reflections and diffractions, S-S wave reflections and diffractions, P-S converted wave

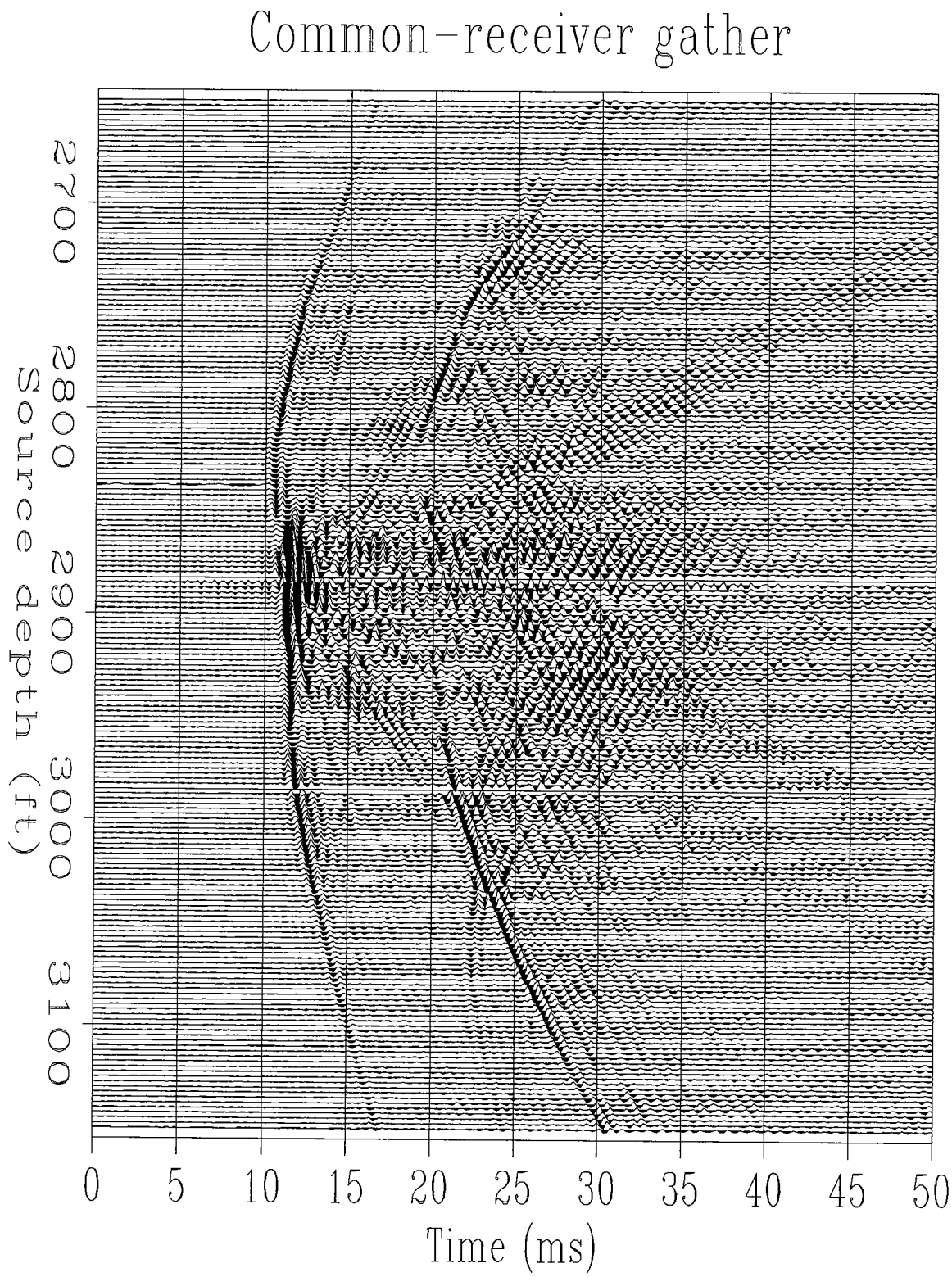

Figure 1: A unprocessed common receiver gather. The receiver is at a depth of 2880 ft in the receiver well.

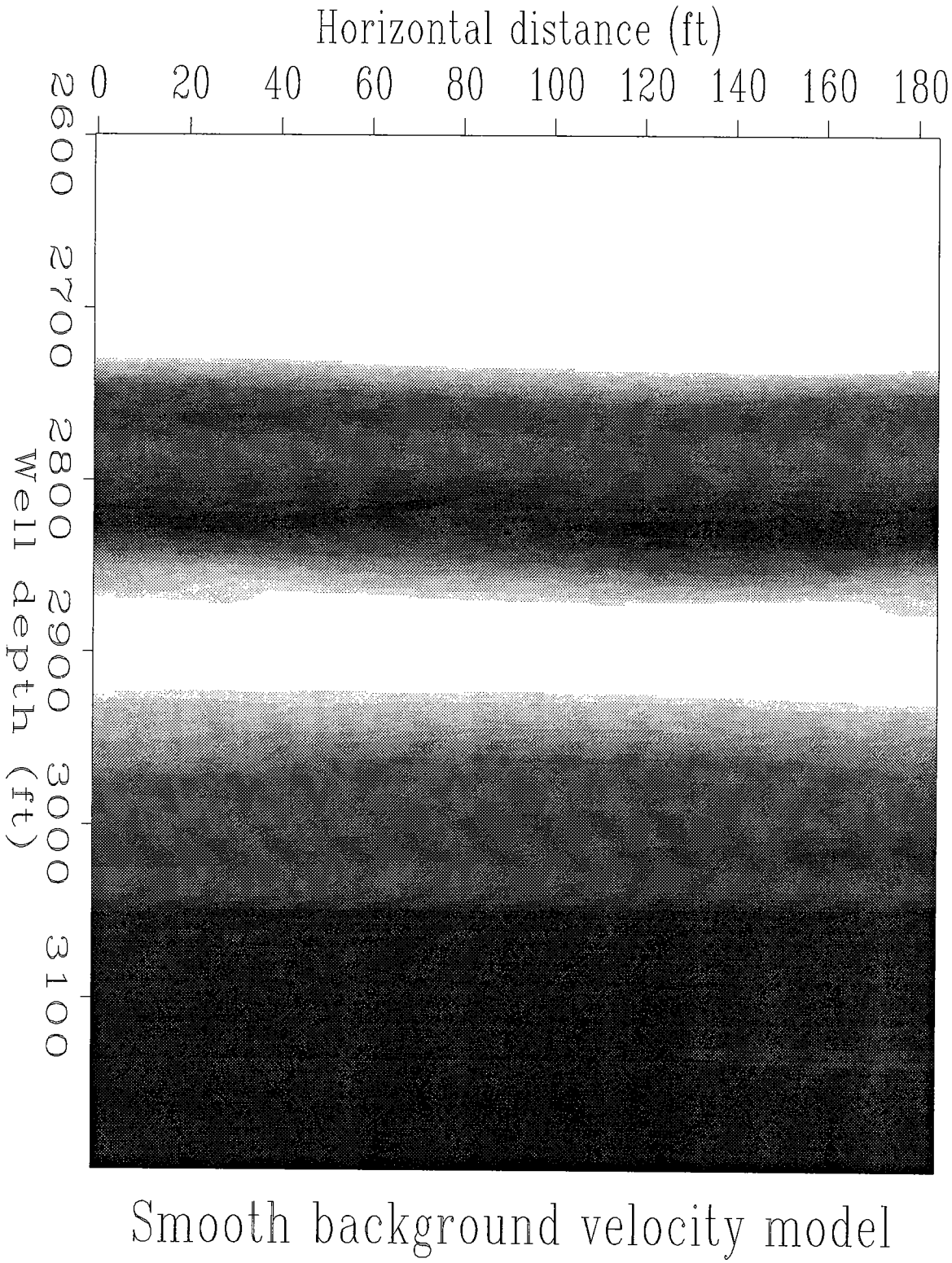

Figure 2: A P-wave smooth background velocity model used as the background model of migration. White (black) means low (high) velocity.

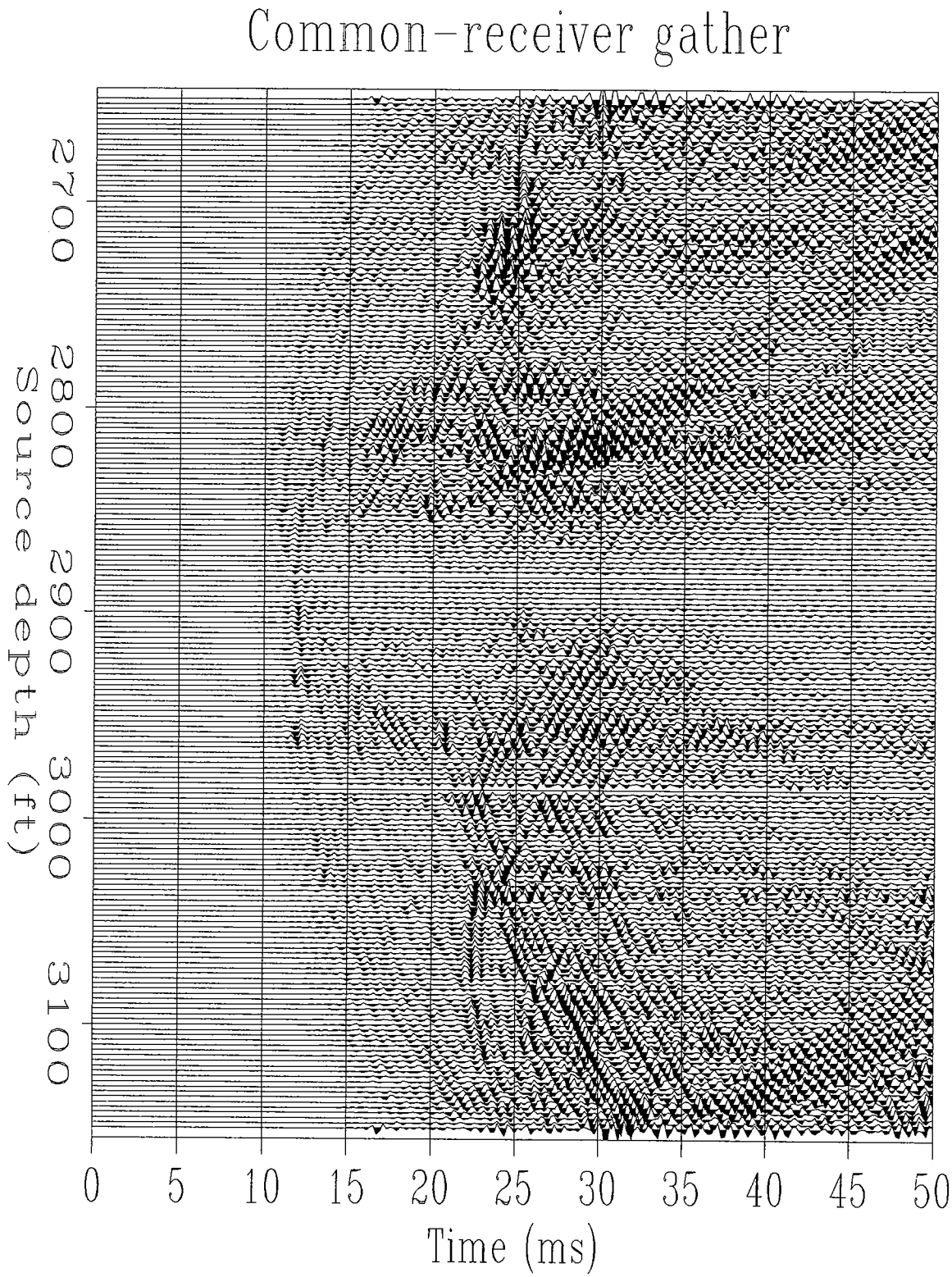

Figure 3: A common receiver gather corresponding to that of Figure 1. The direct P-wave and S-wave have been attenuated by processing in common offset sections.

reflections and diffractions and transmissions, S-P converted wave reflections and diffractions and transmissions. These wavefields are considered as scattered wavefields. And they are used for imaging.

The P-P wave and S-P wave images as a group are produced by one-pass migration. And the P-S and S-S wave images as a group are produced by a separate pass. During the migration process, we backpropagate the data of Figure 3 as P waves and apply two imaging conditions corresponding to P and S waves; we obtain the P-P wave and S-P wave images. And during another pass of migration, we backpropagate the data of Figure 3 as S waves and apply two imaging conditions corresponding to P and S waves; we obtain the P-S wave and S-S wave images. Note that the P-S and S-P converted transmissions are used together with their reflections and transmissions for imaging.

PRELIMINARY RESULTS

Figure 4 is the P-P wave migration image corresponding to the common receiver gather of Figure 3. The prestack migration impulse response, that prestack migration spreads one data point into a whole ellipse, is obvious on this image. Figure 5 is the S-P wave image, Figure 6 the P-S image, Figure 7 the S-S image corresponding to the data of Figure 3.

We migrate all the common receiver gathers. Figure 8 is the P-P wave stack image produced by brute force stacking all the 178 individual P-P wave images. Even though this image shows the main reflection events, it is dominated by different noises. Further interpretation is impossible.

POST-MIGRATION SIGNAL/NOISE SEPARATION

After the prestack migration on all the common receiver gathers, we obtain an image cube. In a constant velocity medium, the prestack migration impulse response is one data point spreads into an ellipse with the source and receiver locations as the loci. Based on the idea that reflection events should be stable but the migration responses of noises are variant as incidence angle changes, we perform geometrical incidence angle transform on the image cube. The geometrical incidence angle is defined as the angle between the incidence straight ray path linking an image point to the source (or receiver) and the vertical line through that image point. The dips of reflection events are invariant in different common incidence angle sections. The noise responses have roughly constant dip in a common incidence angle section. And the dip angle is 90 degrees minus the absolute value of the incidence angle. We apply 2-D dip filters on the common incidence angle migration images to remove noises. We then select the common incidence angle migration images with high signal/noise ratios to stack. In a crosswell survey geometry, the geometrical reflections that can be received correspond to incidence angles roughly from 20 degrees to 70 degrees. So

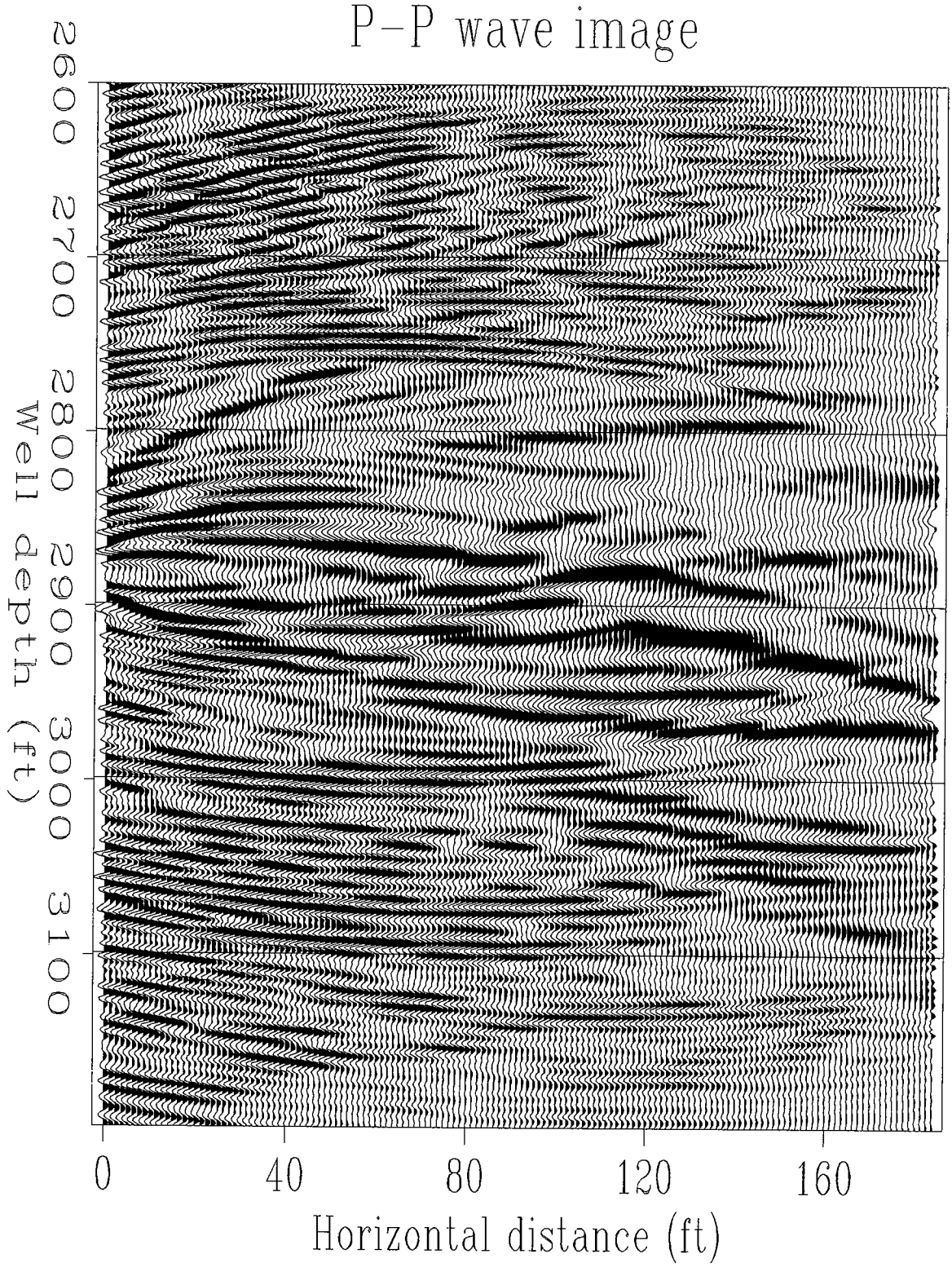

Figure 4: The P-P wave migration image corresponding to the data of Figure 3. Notice the prestack migration ellipse.

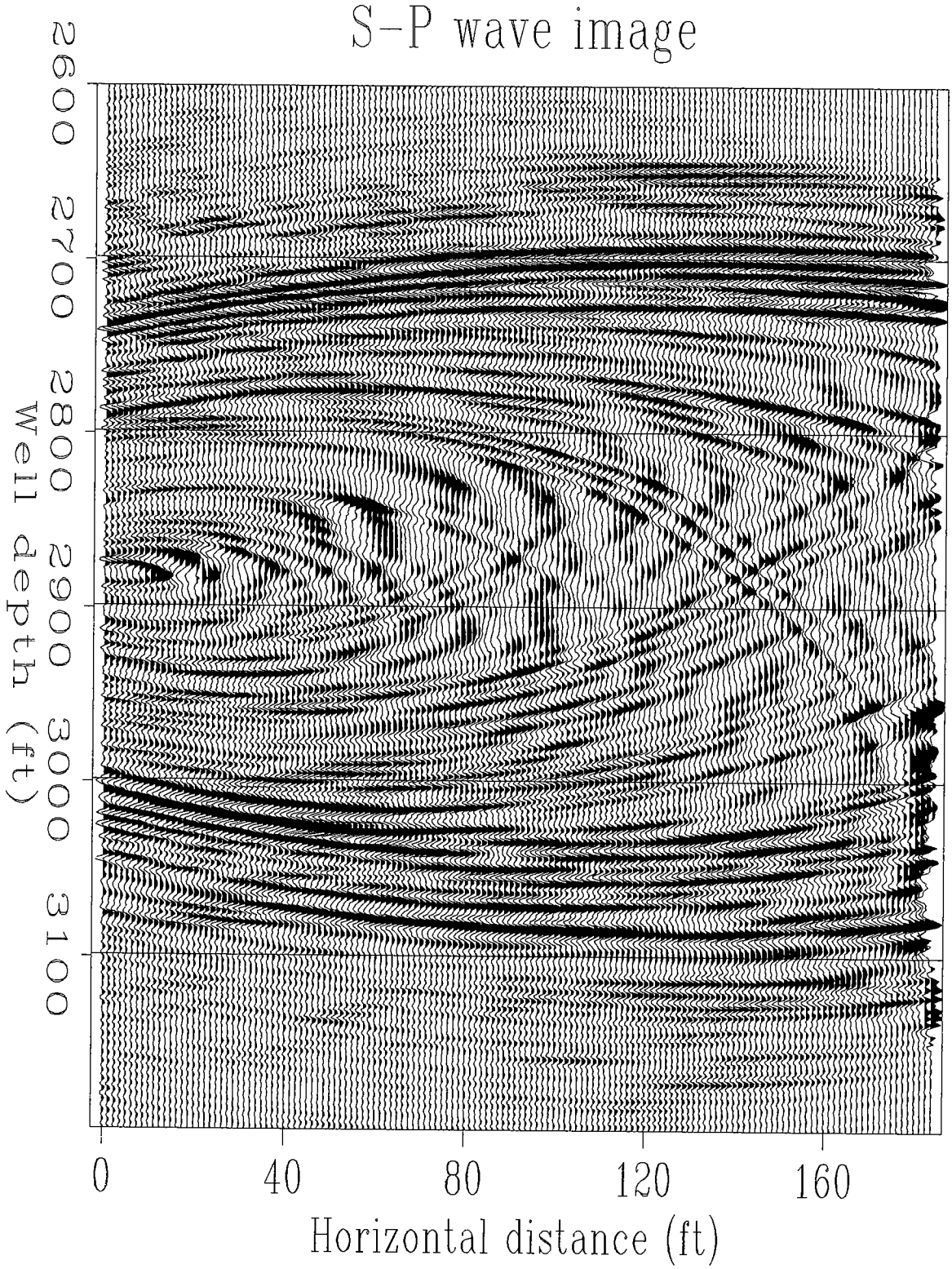

Figure 5: The S-P wave migration image corresponding to the data of Figure 3.

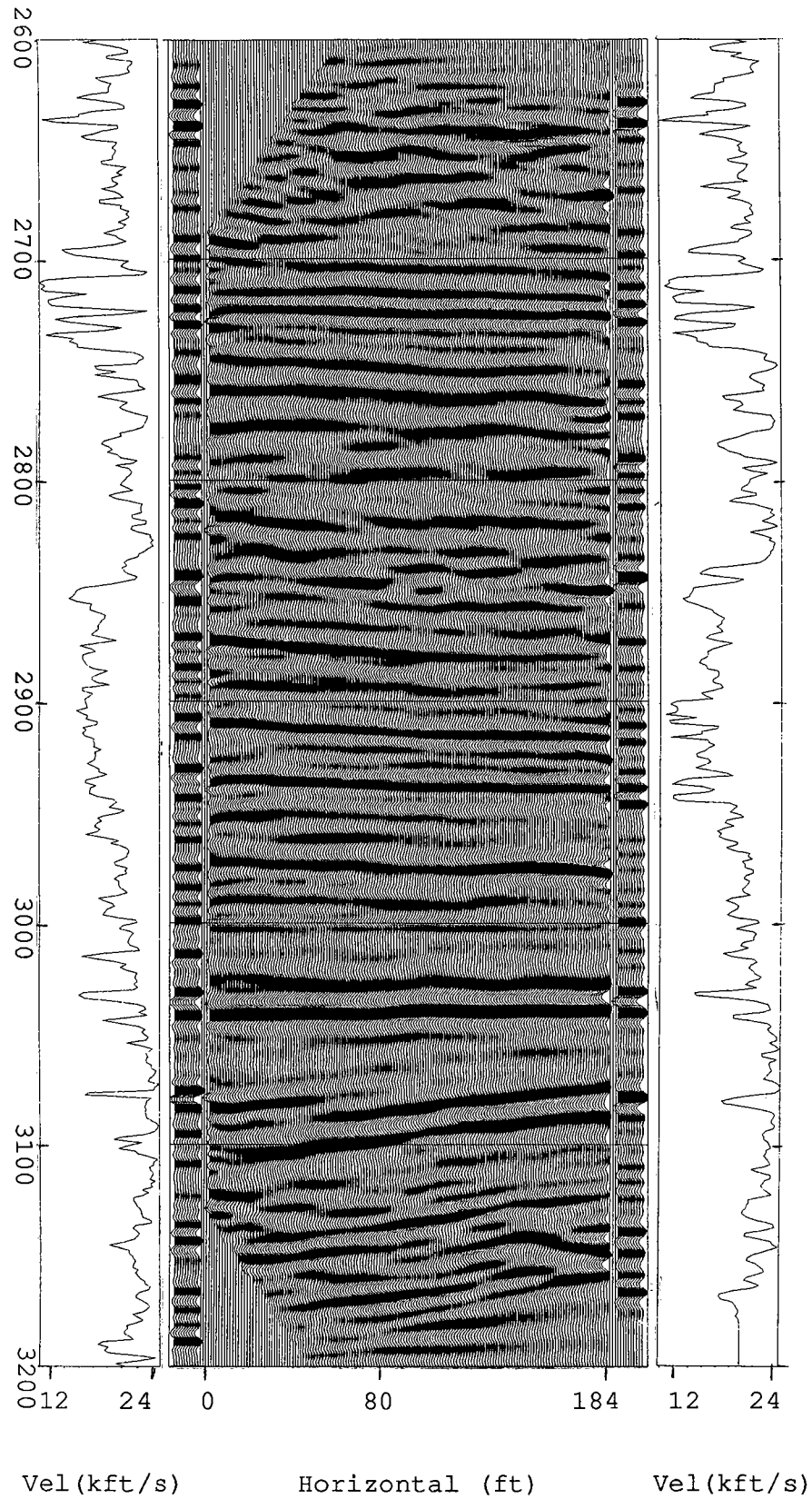

Figure 9: P-P wave image, P wave sonic logs, and synthetics.

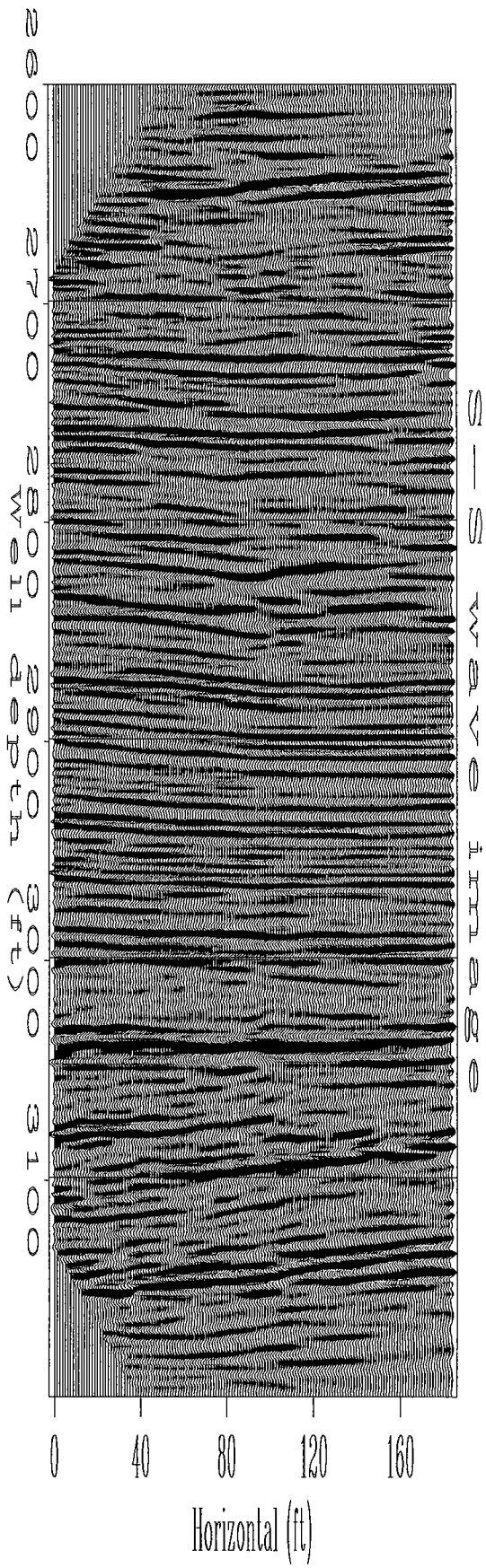

Figure 10: Final S-S wave image.

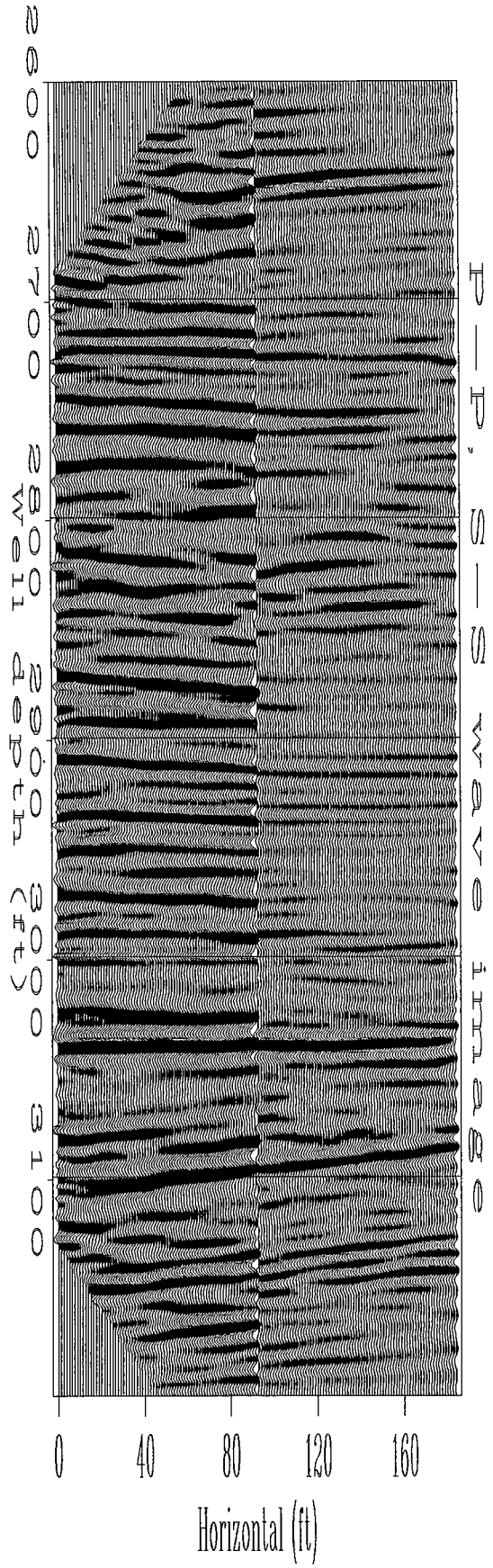

Figure 11: The left half is P-P wave image, and the right half is S-S wave image.

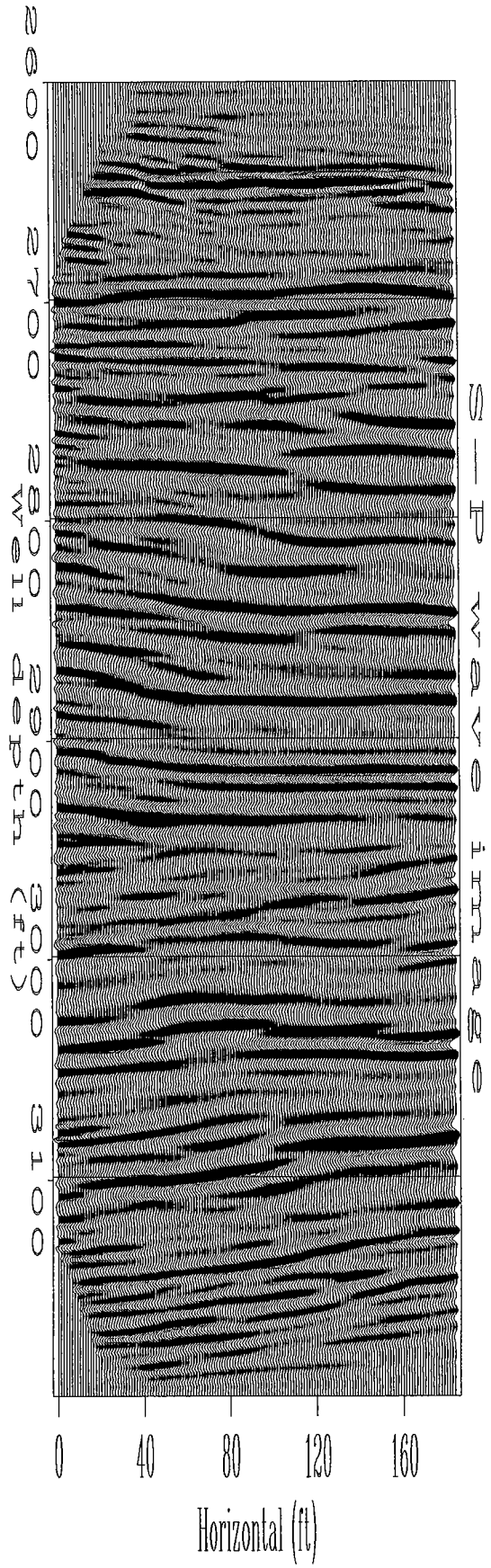

Figure 12: Final S-P wave image.

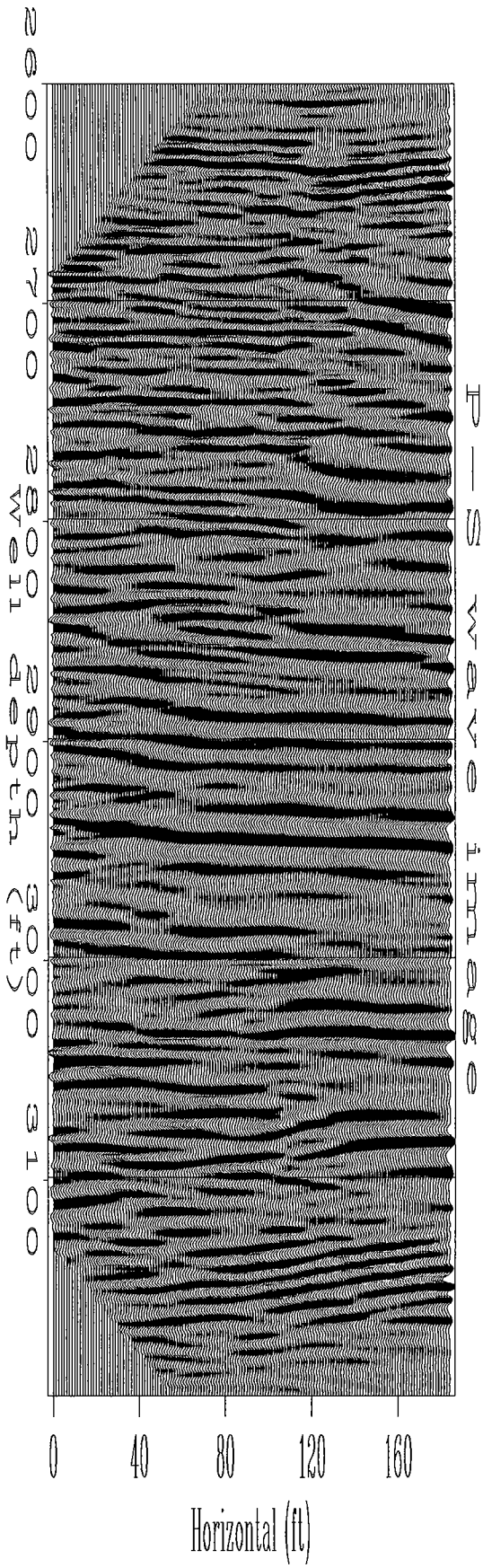

Figure 13: Final P-S wave image.

The sonic logs above depth of 2700 ft are similar at both wells. At the depth of 2700 ft is a time unconformity. The P-P and S-S images show dipping events at depth of 2670 ft, but the S-P and P-S images do not. These dipping events are not likely due to geology, but possibly are migration edge artifacts.

To better depict the reservoir zone between depth of 2800 ft and 3000 ft, we show the enlarged P-P image in Figure 14 and S-S image in Figure 15.

PROCESSING SEQUENCE FOR FIELD DATA

In summary, our processing sequence is:

1. 3-D to 2-D amplitude adjustment by a time scaling of $\sqrt{t}$.
2. Remove direct arrival in common offset sections by mixing and subtraction (Rector et al., 1992).
3. Prestack migration on the common shot (or receiver) gathers.
4. Geometrical incidence angle transform on the migration image cube (Lazaratos, 1993).
5. Dip filtering on the common incidence angle sections to remove noise.
6. Stack the optimal common incidence angle sections.
7. Wavenumber bandpass filtering to the available signal wavenumber band.
8. AGC the image of (7) to enhance the weak reflection events for structure interpretation.

CONCLUSIONS

Crosswell seismic data recorded with our acquisition system contain a rich variety of elastic wave modes, P-P, P-S, S-P, and S-S, the bandwidths of which range from a few hundred Hertz up to a few thousands Hertz. It has been shown in this paper that proper prestack reverse time migration, filtering, and stacking of crosswell seismic data give high-quality reflectivity images of multi-elastic wavemodes of P-P, P-S, S-P, and S-S. The detailed structure around a 100 ft reservoir has been successfully imaged, with resolution of a few feet. A good tie was achieved with sonic logs recorded at both wells.

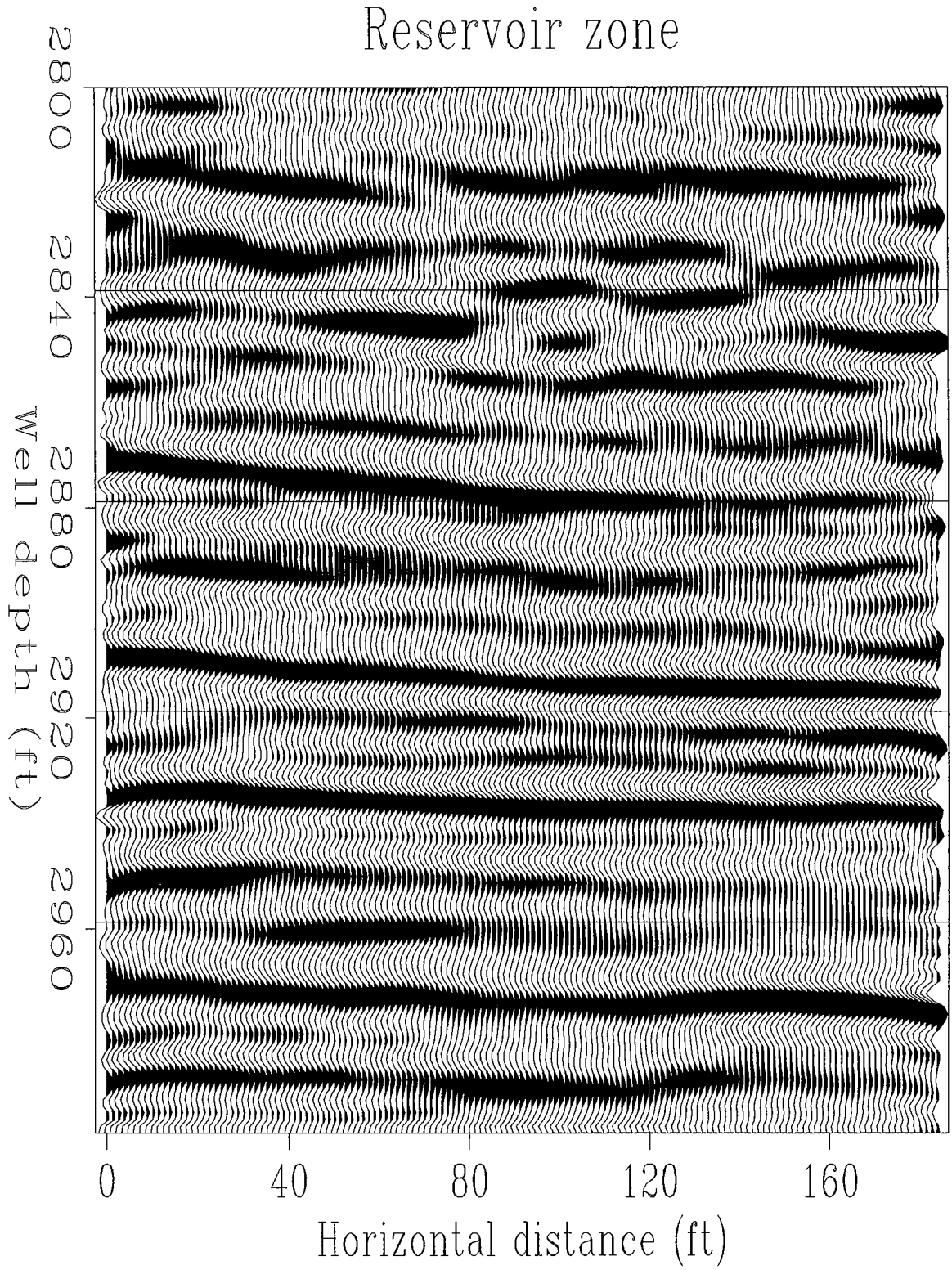

Figure 14: Enlarged P-P image at the reservoir zone.

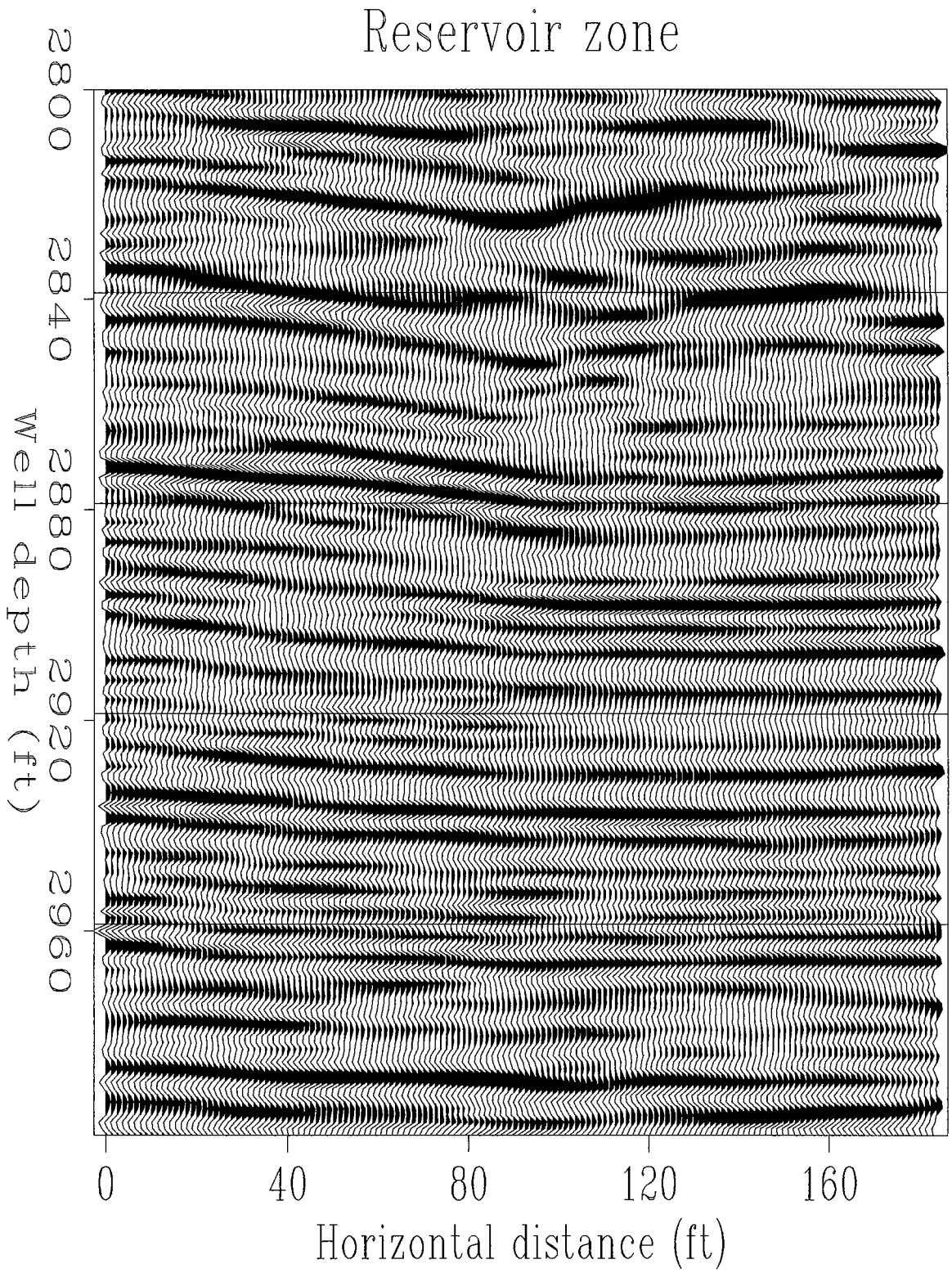

Figure 15: Enlarged S-S image at the reservoir zone.

REFERENCES

Chang, W. F., and McMechan, G. A., 1986, Reverse-time migration of offset vertical seismic profiling data using the excitation-time imaging condition: Geophysics, **51**, 67–84.

Claerbout, J. F., 1985, Imaging the Earth's Interior: Blackwell Scientific.

Harris, J. M., 1992, High resolution imaging of a West Texas Carbonate reservoir: Part 1 – Project review and data acquisition: STP–**3**, paper-A.

Hu, L. Z., McMechan, G. A., and Harris, J. M., 1988, Acoustic pre-stack migration of cross-hole data: Geophysics, **53**, 1015–1023.

Lazaratos, S. K., 1993, Crosswell reflection imaging: Ph. D. dissertation: Dept. of Geophysics, Stanford University.

McMechan, G. A., 1983, Migration by extrapolation of time-dependent boundary values: Geophys. Prosp., **31**, 413–420.

Mo, L., 1992, Gaussian beam migration: SEP–**75**, 65–84.

Mo, L., and Harris, J. M., 1993a, Migration of crosswell seismic data: Synthetic acoustic case: STP–**4**, paper-K.

Rector, J., Lazaratos, S., Harris, J., and Van Schaack, M., 1992, High resolution crosswell imaging of a West Texas Carbonate reservoir: Part 3 – Wavefield separation: 62nd SEG conference, 45-48, New Orleans.

Van Schaack, M., 1992, High resolution crosswell imaging of a West Texas Carbonate reservoir: Part 3 – traveltime tomography: STP–**3**, paper-C.

Van Trier, J., and Symes, W. W., 1990, Upwind finite-difference calculation of traveltimes: SEP–**65**, 41–58.